

Electronic and magnetic properties of spiral spin-density-wave states in transition-metal chains

M. Tanveer

Institut für Theoretische Physik, Universität Kassel, Heinrich Plett Straße 40, 34132 Kassel, Germany

P. Ruiz-Díaz

Max-Planck Institut für Mikrostrukturphysik, Weinberg 2, D-06120 Halle, Germany

G. M. Pastor

Institut für Theoretische Physik, Universität Kassel, Heinrich Plett Straße 40, 34132 Kassel, Germany

(Received 23 March 2016; revised manuscript received 8 July 2016; published 6 September 2016)

The electronic and magnetic properties of one-dimensional (1D) 3d transition-metal nanowires are investigated in the framework of density functional theory. The relative stability of collinear and noncollinear (NC) ground-state magnetic orders in V, Mn, and Fe monoatomic chains is quantified by computing the frozen-magnon dispersion relation $\Delta E(\vec{q})$ as a function of the spin-density-wave vector \vec{q} . The dependence on the local environment of the atoms is analyzed by varying systematically the lattice parameter a of the chains. Electron correlation effects are explored by comparing local spin-density and generalized-gradient approximations to the exchange and correlation functional. Results are given for $\Delta E(\vec{q})$, the local magnetic moments $\vec{\mu}_i$ at atom i , the magnetization-vector density $\vec{m}(\vec{r})$, and the local electronic density of states $\rho_{i\sigma}(\varepsilon)$. The frozen-magnon dispersion relations are analyzed from a local perspective. Effective exchange interactions J_{ij} between the local magnetic moments $\vec{\mu}_i$ and $\vec{\mu}_j$ are derived by fitting the *ab initio* $\Delta E(\vec{q})$ to a classical 1D Heisenberg model. The dominant competing interactions J_{ij} at the origin of the NC magnetic order are identified. The interplay between the various J_{ij} is revealed as a function of a in the framework of the corresponding magnetic phase diagrams.

DOI: [10.1103/PhysRevB.94.094403](https://doi.org/10.1103/PhysRevB.94.094403)**I. INTRODUCTION**

The magnetism of low-dimensional systems remains, despite its long history, one of the most important current challenges in condensed-matter physics. Together with the traditional ultrathin films and multilayers, a variety of new nanostructured materials including small particles, nanowires, and nanohybrids have recently gained considerable attention in both basic and applied science [1–8]. Understanding their behavior is not only challenging from a fundamental perspective but also considerably important in view of developing novel technologies [1–4,6–9]. Potential applications may be found, for example, in the fields of nonvolatile random-access memories, read-write heads, high-density storage media, and spin-electronic devices. Many experimental and theoretical studies have already shown that reducing the dimensionality of a macroscopic material leads to magnetic properties, which are either strongly modified or have simply no equivalent in the bulk. One-dimensional (1D) systems in particular are known to display a variety of remarkable effects such as enhanced spin and orbital moments, giant magnetic anisotropy [1,10], long-range atomic ordering [11,12], noncollinear (NC) spin arrangements [13–16], quantum confinement [17], and local moment self-alignments [18,19]. Therefore, 1D nanostructures define a fascinating research area in which a number of technological, experimental, and theoretical interests converge.

In past years, remarkable advances towards the practical realization of ideal 1D geometries have been achieved by using diffusion-controlled aggregation [1,6] and atomic manipulation techniques, such as scanning tunneling microscopy (STM) [20–24]. In this way new experimental opportunities to tailor magnetism in low dimensions have been opened. The study of complex chiral magnetic arrangements, such

as spiral and vortex spin states, has attracted considerable attention in this context [23–29]. These complex NC magnetic orders are often the result of competing exchange interactions, for example, when antiferromagnetic (AF) couplings are frustrated in nonbipartite lattices, or when ferromagnetic (FM) and AF couplings coexist at different interatomic distances [30]. More subtle effects induced by spin-orbit interactions are observed in extended 2D vortex structures such as magnetic skyrmions [26–29], which are stabilized by the asymmetry of the exchange-coupling tensor (Dzyaloshinskii-Moriya coupling) [31].

Competing magnetic interactions J_{ij} between the local magnetic moments at different atoms i and j have been found in a wide variety of low-dimensional systems, even for elements that exhibit a strong tendency towards collinear ferromagnetic order in the bulk. Density functional theory (DFT) with the standard approximations to exchange and correlation has been able to describe spiral spin-density wave (SDW) states in a variety of itinerant-electron magnetic materials. This includes, in particular, Cr, γ -Fe, and U three-dimensional crystals [32–35], Fe monolayers [36,37], and transition-metal (TM) nanowires [14–16,38–42]. Stable spiral arrangements have been predicted for V, Mn, and Fe 1D chains, while collinear structures are favored in the case of Cr, Co, and Ni wires [14–16]. In addition, the effects of wire-substrate hybridizations have been investigated for Mn, Fe, and Ni chains on nonmagnetic surfaces [16,43].

The electronic and magnetic properties of SDW states are a subject of considerable interest, not only from the fundamental perspective of magnetism. They are also very important in view of integrating low-dimensional systems in more complex nanostructures, such as deposited stripes or

chain arrays. The stability of NC magnetism in TM chains has already been studied in some detail [14–16,41]. However, comparatively little is known so far about the signatures of spiral order on other properties, such as the electronic structure or the spin-polarized density distribution, which are of great experimental and theoretical interest. It is one of the goals of this paper to investigate these properties from a local perspective in the framework of DFT. To this aim, the single-particle local densities of electronic states $\rho(\varepsilon)$ and the magnetization-vector density $\vec{m}(\vec{r})$ of 1D TM systems are determined as functions of the SDW vector \vec{q} , by taking V, Mn, and Fe chains as representative examples. The effects of electron correlations on the stability of SDWs are explored by comparing local and gradient-corrected approximations to the exchange and correlation (XC) energy functional. The importance of the local environment of the atoms is quantified by varying the lattice parameter a of the chains and by analyzing the resulting changes in the effective magnetic interactions J_{ij} between the local moments. The interplay between the different couplings J_{ij} and the global magnetic behavior of the chains are interpreted in the framework of the phase diagram of a classical Heisenberg model.

The remainder of the paper is organized as follows. In Sec. II the modelization of SDW states and the most important computational details are described. In Sec. III the stability of SDWs in V, Mn, and Fe wires is investigated for different lattice parameters, by calculating the corresponding frozen-magnon dispersion relations as a function of the wave number q . The effective exchange interactions $J_{0\delta}$ between the local moments $\vec{\mu}_0$ and $\vec{\mu}_\delta$ are obtained as a function of the intermoment separation δ . In addition, the associated magnetization-vector density $\vec{m}(\vec{r})$ is analyzed for representative values of q . Section IV discusses the relative stability of the different types of collinear and noncollinear magnetic orders from a local perspective. The phase diagram of the 1D classical Heisenberg model is obtained as a function of the dominant first-, second-, and third-nearest-neighbor (NN) interactions. Following the evolution of the *ab initio* results for $J_{0\delta}$ within these phase diagrams, as a function of the lattice parameter a , provides new insights on the development of NC instabilities. In Sec. V the local densities of states in spiral states having different q are discussed: from the FM state ($q = 0$) over the NC orders to the AF state ($q = \pi/a$). Results for Mn and Fe chains are contrasted. Finally, Sec. VI summarizes our conclusions and points out some interesting future research directions.

II. THEORETICAL BACKGROUND

We consider 1D periodic chains placed along the z axis and having a lattice parameter a . Assuming for simplicity that all local moments share the same polarization plane, the spin-spiral states can be characterized by the wave vector $\vec{q} = [0,0,q]$ along the wire axis, where $q = 2\pi/Na$ is the wave number and N is the number of atoms in a real space period (see Fig. 1). The collinear orders correspond to $q = 0$ (FM) and $q = \pi/a$ (AF). The electronic calculations can thus be performed by using a supercell approach, constraining the direction of the local magnetic moment μ_l at each atom l in the supercell. For each considered $N \leq 16$, all the wave numbers q compatible with the cell periodicity are taken into

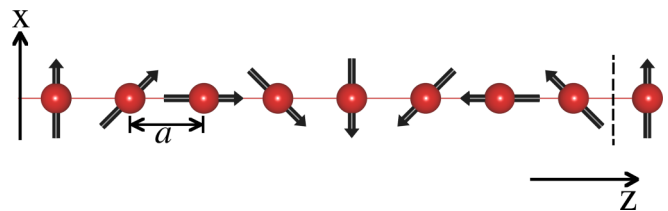


FIG. 1. Illustration of a spiral spin-density wave having a wave vector $\vec{q} = (0,0,\pi/4a)$ and local magnetic moments within the xz plane. The size of the supercell is indicated by the vertical dashed line.

account (i.e., $q = 2\pi l/Na$ with $0 \leq l < N$). The supercell dimensions in the directions perpendicular to the wire axis are chosen large enough (typically 16 Å) so as to avoid any spurious interactions between the periodic replicas.

The calculations have been performed in the framework of Hohenberg-Kohn-Sham's DFT as implemented in the Vienna *ab initio* simulation package (VASP) [44]. The considered XC energy functional is mainly the generalized-gradient approximation (GGA) introduced by Perdew and Wang [45]. In addition, calculations have been performed by using the local-density approximation (LDA) in order to gain some insight into the role of electron correlations on the stability of SDWs. In this case we use the Ceperly-Alder parametrization, together with the Vosko-Wilk-Nusair correlation [46,47]. The spin-polarized Kohn-Sham (KS) equations are solved in an augmented plane-wave basis set, taking into account the interaction between valence electrons and ionic cores by means of the projector-augmented-wave method [48]. Only the 4s, 4p, and 3d orbitals are treated as valence electrons. The KS wave functions are expanded in the interstitial region by using plane waves with a cutoff energy $E_{\max} = 500$ eV. The integrations in the Brillouin zone (BZ) are performed by applying the Monkhorst-Pack scheme with a k mesh [49] having $1 \times 1 \times N_k$ points, where $N_k = 30$ for $N = 4$ and $N_k = 12$ for $N = 10$, for example. The accuracy of this choice has been explicitly checked by considering higher cutoff energies and denser k meshes for representative examples. The convergence criterion for the electronic energy has been set to 10^{-5} eV, which is much smaller than all relevant energy variations in this work. In the case of lattice parameter relaxations, convergence is assumed when the forces on each atom are below 10^{-2} eV/Å. This corresponds to a total energy accuracy better than 1 meV/atom, which is sufficient for the present purposes.

Metallic systems often show very rapid changes in the states close to the Fermi level ε_F as a function of the spin-polarized input density. This may cause a poor convergence of important physical properties, such as the total energy or the local magnetic moments. Therefore, a smearing of the KS energy levels is introduced in order to improve the numerical stability. In this work we use a Gaussian smearing with a width $\sigma = 0.02$ eV, a value that ensures that the smearing contribution to the total energy is less than 10^{-4} eV/atom.

The NC magnetic calculations are performed within a fully unconstrained density functional formalism, in which the density matrix $n_{\alpha\beta}(\vec{r})$ is the fundamental variable and the KS orbitals are spin- $\frac{1}{2}$ spinors [50]. The charge density $n(\vec{r})$ is

then given by the trace

$$n(\vec{r}) = \sum_{\alpha} n_{\alpha\alpha}(\vec{r}), \quad (1)$$

and the magnetization density by

$$\vec{m}(\vec{r}) = \sum_{\alpha\beta} n_{\alpha\beta}(\vec{r}) \vec{\sigma}_{\alpha\beta}, \quad (2)$$

where $\vec{\sigma}_{\alpha\beta}$ stands for the matrix elements of the vector of Pauli matrices $\vec{\sigma} = (\sigma_x, \sigma_y, \sigma_z)$. Further details on the implementation may be found in Ref. [50]. The constraints in the direction of the local magnetic moment μ_l at each atom l of the supercell are imposed by means of a penalty function, as proposed by Haynes and Payne [51]. Alternative methods have been formulated in Refs. [52] and [53].

III. EFFECTIVE MAGNETIC INTERACTIONS FROM FIRST PRINCIPLES

In this section we determine the effective magnetic interactions between the local moments and the stability of SDW states in V, Mn, and Fe chains from a first-principles perspective. To this aim we calculate the frozen-magnon dispersion relation $\Delta E(q) = E(q) - E(0)$ as a function of the wave number q . The role of structural relaxations and of the local atomic environment of the nanowires is studied by varying the lattice parameter a .

A. V chains

In order to quantify the effects of electron correlations on the SDW formation, we compare the results of different approximations to XC. In Fig. 2 the magnon-dispersion relations of V wires obtained by using the GGA and the LDA are shown [45–47]. As already reported in a previous study [14], the GGA yields a ferromagnetic ground state for $a \geq 2.6$ Å, while for $a \leq 2.55$ Å the most stable arrangement is a SDW. The energy ΔE gained upon the formation of the spiral state with the optimal $q = q_{\min}$ is usually rather

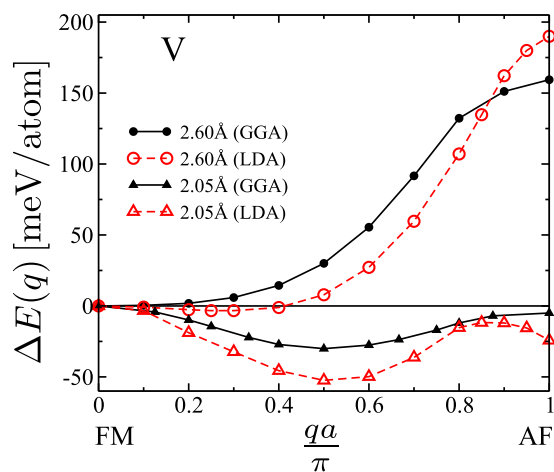


FIG. 2. Frozen-magnon dispersion relation $\Delta E(q) = E(q) - E(0)$ of V chains calculated by using the spin-polarized GGA and LDA to the exchange and correlation functional. Results are given for two representative lattice parameters $a = 2.05$ Å and $a = 2.60$ Å.

small. For instance, for $a = 2.55$ Å ($a = 2.05$ Å) we obtain $\Delta E = -2$ meV/atom ($\Delta E = -30$ meV/atom) at $q_{\min} \simeq \pi/4a$ ($q_{\min} \simeq \pi/2a$). This refers to the difference with respect to the most stable collinear order, i.e., the FM order. It should be also noted that for large a the optimal spiral states are significantly more stable than the AF state ($q = \pi/a$). For example, $E(\pi/a) - E(q_{\min}) \simeq 120$ meV/atom for $a = 2.55$ Å (see also Ref. [14]).

Using the LDA one obtains qualitatively similar q dependencies. However, the stability of NC spin configurations is clearly stronger in this case (see Fig. 2). For instance, in the LDA a shallow minimum is found in $\Delta E(q)$ at $q \simeq \pi/5a$ already for 2.6 Å, whereas the GGA predicts a FM ground state. The quantitative differences between LDA and GGA results become even more important for short interatomic distances. For example, for $a = 2.05$ Å we obtain $\Delta E_{\text{GGA}}(q_{\min}) = -30$ meV/atom, while $\Delta E_{\text{LDA}}(q_{\min}) = -50$ meV/atom. This can be interpreted as a stronger tendency of the LDA to favor electron delocalization and hybridization, which enhances the importance of the second-NN exchange interaction J_{02} , relative to the first-NN coupling J_{01} . In fact, the interplay between the different J_{ij} found with the LDA for a given lattice parameter a is similar to what is found with the GGA at a somewhat larger a . It should be noted, however, that in other TM chains—for example, in Mn chains—the differences between the LDA and GGA frozen-magnon dispersion relations are very small. Mn wires are discussed in the following section. A comparison between LDA and GGA results for Mn chains may be found in the Supplemental Material [54].

In order to understand the magnetic properties of spiral states, it is useful to take a local perspective and analyze the spatial distribution of the magnetization vector density $\vec{m}(\vec{r})$, not only inside of the Wigner-Seitz (WS) spheres of each atom, but also in the interstitial and outer regions. In Fig. 3 results are shown for $\vec{m}(\vec{r})$ of a V chain having a $\pi/2$ spiral state. One observes that the directions of $\vec{m}(\vec{r})$ are almost perfectly parallel for all \vec{r} within the WS sphere of any given atom i . It is also in this localized regions that the far largest contribution to the local moments μ_i is obtained. These results confirm the strong stability of the local moments and the idea of attaching a well-defined $\vec{\mu}_i$ to each atom, as expected from the strong exchange interactions within the 3d shell (first Hund rule). In a direction perpendicular to the wire (e.g., the x direction) the spill-off spin density preserves a parallel alignment to the corresponding atom as it vanishes with increasing $|x|$. This is consistent with the experimental observation of spiral SDWs in spin-polarized scanning tunneling experiments, since the spilled-off magnetization density reflects the magnetic order of the local 3d moments. Significant deviations from collinearity [i.e., $\nabla(\vec{m}/m) \neq 0$] are found only in the very narrow interstitial regions between the atoms (typically 0.5 Å wide). It is in these sort of subatomic “domain walls” that the actual rotation of $\vec{m}(\vec{r})$ from atom to atom takes place. Notice that the magnitude of the magnetization density $m(\vec{r})$ is strongly reduced in the interatomic domain walls. For example, at the midpoint between two atoms we find $m(\vec{r}) \simeq 25 \times 10^{-3} \mu_B/\text{Å}^3$, while near the atoms we find $125 \times 10^{-3} \mu_B/\text{Å}^3$. This can be interpreted as the result of the

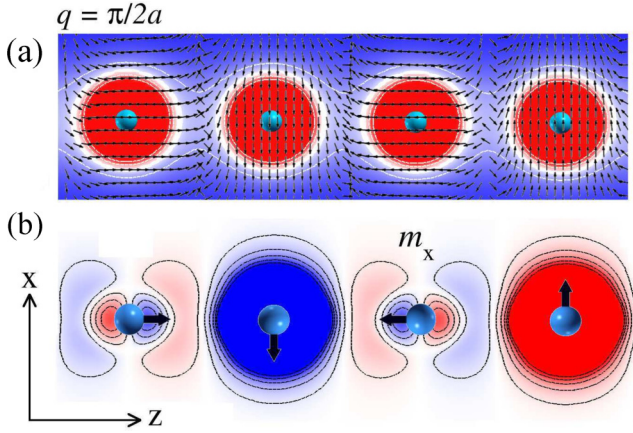


FIG. 3. Magnetization density distribution $\vec{m}(\vec{r})$ of a V chain in a spiral SDW state having $\vec{q} = (0, 0, \pi/2a)$, where $a = 2.55 \text{ \AA}$ is the lattice parameter. Results obtained in the GGA are given for \vec{r} within the xz plane, as well as for x and z components of \vec{m} , since the xz plane contains both the chain (along z) and the local moments $\vec{\mu}_i$. In (a) the color saturation (grayscale) indicates the absolute value of the magnetization density $m(\vec{r})$, so that light (strong) colors correspond to low (high) values of $m(\vec{r})$. The small arrows represent the direction of $\vec{m}(\vec{r})$ at the corresponding position. In (b) the contour plot of the component $m_x(\vec{r})$ of the magnetization density vector is shown. Positive (negative) values of m_x are indicated in red (blue) and the absolute value $|m_x|$ is roughly proportional to the color saturation. The arrow at each atom i indicates the direction of the local magnetic moment $\vec{\mu}_i$.

interplay between kinetic and exchange energies, the former tending to reduce the spin polarization in the presence of noncollinearity.

A complementary perspective of $\vec{m}(\vec{r})$ is adopted in Fig. 3(b). Here we show the contour plots of the component $m_x(\vec{r})$ of the magnetization vector density along the direction \hat{x} , which is perpendicular to the chain. One observes that $m_x(\vec{r})$ is large and nearly isotropic around the atoms having $\vec{\mu}_i$ parallel or antiparallel to \hat{x} . These are the second and fourth atoms in Fig. 3. In contrast, $m_x(\vec{r})$ is very small and antisymmetric with respect to reflection across the xy plane when $\vec{\mu}_i$ points along \hat{z} . This corresponds to the first and third atoms in Fig. 3. Similar periodic oscillations have been observed in spin-polarized STM measurement on Fe chains on Ir(001) [23].

B. Mn chains

The calculated optimal lattice parameter in free-standing Mn chains is $a = 2.6 \text{ \AA}$ ($a = 2.4 \text{ \AA}$) when a collinear FM (AF) order is assumed. These values are in good agreement with earlier studies [15,16,38,39]. Comparing collinear orders we find that ferromagnetism is more stable for $a \geq 2.6 \text{ \AA}$, while the AF configuration is more stable at shorter bond lengths. This is consistent with previous collinear calculations, which predicted an AF-to-FM transition with increasing interatomic distance [11]. The frozen-magnon dispersion relations $\Delta E(q)$, shown in Fig. 4(a) for different values of a , demonstrate the stability of the spiral SDWs. Similar results have been

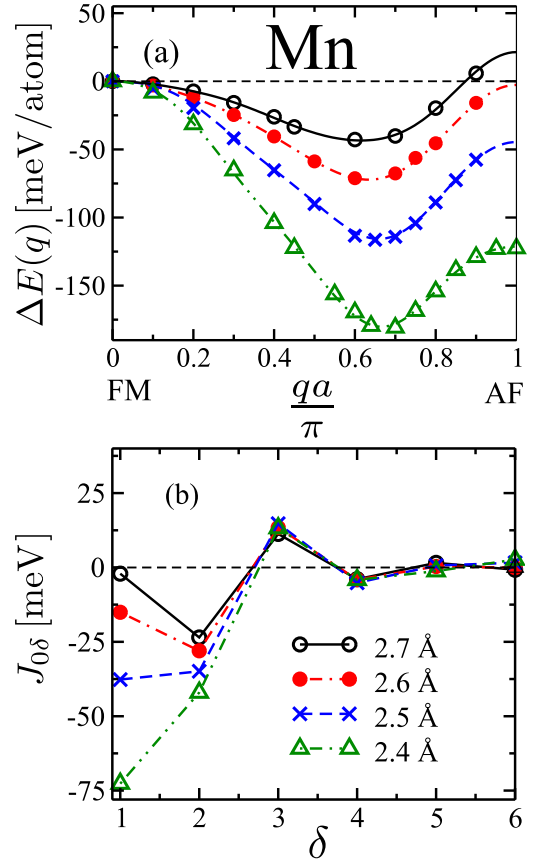


FIG. 4. Frozen-magnon dispersion relations and effective exchange interactions in Mn chains. The symbols in (a) are the *ab initio* results for $\Delta E(q) = E(q) - E(0)$, while the curves show the corresponding fits obtained in the framework of a classical Heisenberg model [Eq. (3)]. The derived exchange interactions $J_{0\delta}$ between a local moment $\vec{\mu}_0$ at atom $i = 0$ and its δ th-nearest neighbor $\vec{\mu}_\delta$ are shown in (b) as a function of δ . The considered values of the lattice parameter a are indicated in the inset.

reported in Ref. [15]. The optimal wave number $q_{\min} \simeq 0.6$ is approximately the same for all considered NN distances. For $a = 2.6 \text{ \AA}$, the spiral configuration is 72 meV/atom (68 meV/atom) more stable than the collinear FM (AF) order. Decreasing a tends to further stabilize the SDWs, while larger a weakens the NC magnetic order. The SDW with the minimum energy is 176 meV/atom more stable than the FM state. Nevertheless, upon stretching the NN bonds ($a = 2.7 \text{ \AA}$) this energy difference drops to 50 meV/atom. Our results are also in agreement with the calculations by Schubert *et al.*, which were performed by using a full-potential linearized augmented-plane-wave approach [16]. Interestingly, this study shows that the ground-state magnetic configuration remains a spiral SDW upon deposition of the Mn chains on noble-metal substrates such as Ag(110) or Cu(110).

The interatomic effective exchange interactions J_{ij} allow us to analyze the stability of NC magnetic order from a local perspective. The *ab initio* results can be interpreted by fitting the calculated $\Delta E(q)$ in the framework of the classical 1D

Heisenberg model,

$$H = - \sum_{i=1}^N \sum_{\delta=1}^{\nu} J_{0\delta} \hat{\mu}_i \cdot \hat{\mu}_{i+\delta}, \quad (3)$$

where $\hat{\mu}_i = \vec{\mu}_i / \mu_i$ stands for the unit vector along the local moment at atom i and $\nu = 6$ defines the interaction range within the chain. Positive (negative) values of $J_{0\delta}$ correspond to FM (AF) couplings. The results for $J_{0\delta}$ obtained in this way are shown in Fig. 4(b). First of all, one observes that the dominant magnetic interactions in Mn chains involve up to third-NNs. Remarkably, $|J_{02}|$ is comparable or even larger than $|J_{01}|$ for $a \leq 2.5 \text{ \AA}$. The resulting strong frustration between competing AF interactions is, in fact, at the origin of the NC spin arrangement. Notice, moreover, that J_{01} is strongly affected by changes in the NN distances, while J_{02} and J_{03} are much less sensitive to structural distortions. In particular, J_{03} is almost constant in the considered bond-length range ($2.4 \leq a \leq 2.7 \text{ \AA}$). Comparing the results for different a shows that both $|J_{01}|$ and $|J_{02}|$ decrease with increasing a . This can be qualitatively understood as the result of the reduction of the interatomic hybridizations, which occurs when the separation between the atoms increases. It suggests that J_{01} and J_{02} have a rather local origin. In contrast, the very weak dependence of $J_{0\delta}$ for $\delta \geq 3$ points to a nonlocal coupling mechanism, maybe mediated by the more delocalized sp electrons. A further consequence of the rapid decrease of $|J_{01}|$ with increasing a is that for large NN distances ($a \geq 2.6 \text{ \AA}$) $|J_{02}|$ and $|J_{03}|$ largely dominate. In this case (weak J_{01}) the FM and AF configurations are nearly degenerate (see Fig. 4).

C. Fe chains

In the following we consider Fe chains as an example of TM whose $3d$ band is more than half filled. The stability of SDWs is investigated by calculating the frozen magnon dispersion relation $\Delta E(q)$ in the GGA to DFT. In Fig. 5(a) results are given for different lattice parameters in the range $2.0 \leq a \leq 2.5 \text{ \AA}$. At the equilibrium NN distance $a = 2.25 \text{ \AA}$ the ground-state magnetic order is a spiral SDW having $q_{\min} \simeq \pi/5a$ and an energy $\Delta E(q_{\min}) = -10 \text{ meV/atom}$. This energy gain relative to the FM configuration is somewhat smaller than the value 15.5 meV/atom obtained in Ref. [15] by using a very similar method. Spin-polarized STM measurements show that finite Fe chains on Ir(001) have a stable spin-spiral order when they are attached at one end to a ferromagnetic Co chain. However, the observed SDW number $q^{\text{exp}} = 2\pi/3$ is significantly shorter than the one obtained here for free-standing chains. As in V and Mn wires, the spiral order becomes increasingly stable when the NN distance decreases. This can be interpreted from a local perspective by considering the effective exchange interactions $J_{0\delta}$ between the local moments, which are shown in Fig. 5(b). In the case of Fe, J_{01} and J_{02} are the dominant couplings. The competition between the FM $J_{01} > 0$ and the AF $J_{02} < 0$ explains the qualitative changes in the dispersion relation $\Delta E(q)$, as well as the resulting changes in the relative stability of collinear and noncollinear spin arrangements. For large a (e.g., $a = 2.5 \text{ \AA}$) J_{01} dominates and the FM order is preferred. However, as a decreases J_{01} decreases and $|J_{02}|$ increases [$J_{01} > 0$ and $J_{02} < 0$; see Fig. 5(b)]. This renders

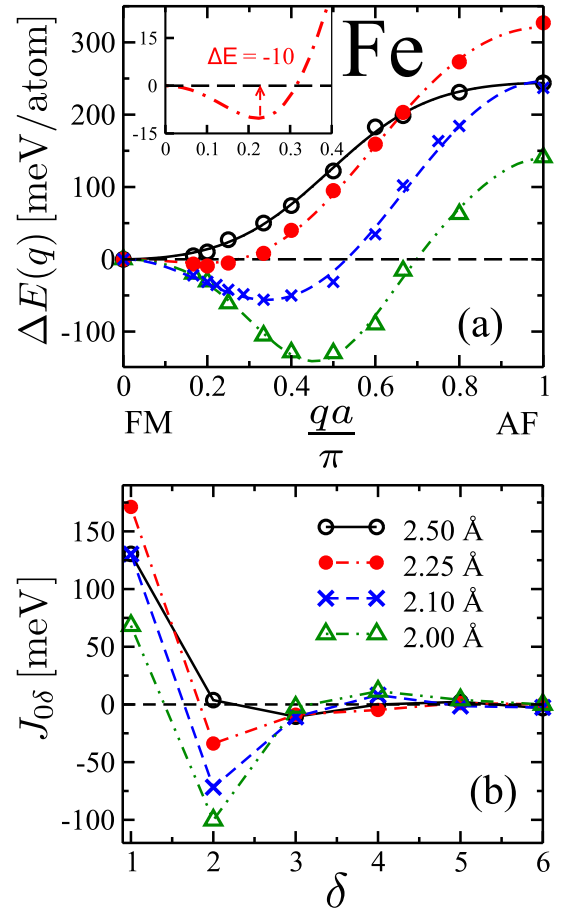


FIG. 5. Frozen-magnon dispersion relations and effective exchange interactions in Fe chains. The symbols in (a) are the *ab initio* results for $\Delta E(q) = E(q) - E(0)$, while the curves show the corresponding fits obtained in the framework of a classical Heisenberg model [Eq. (3)]. The derived exchange interactions $J_{0\delta}$ between a local moment $\vec{\mu}_0$ at atom $i = 0$ and its δ th-nearest neighbor $\vec{\mu}_\delta$ are shown in (b) as a function of δ . Representative values of the lattice parameter a are considered as indicated in the inset.

the FM NN coupling weaker and the AF second-NN stronger, which obviously favors the NC configurations. For example, for $a = 2.1 \text{ \AA}$, J_{01} and J_{02} are comparable and the ground state corresponds to a SDW with $q \simeq 0.35\pi/a$. For even smaller a (e.g., $a = 2.0 \text{ \AA}$) the compensation between J_{01} and J_{02} is such that couplings at larger distances, in particular J_{03} , need to be taken into account in order to identify the actual ground state. Exchange interactions in Fe chains have been reported in Ref. [15] for the equilibrium NN distance.

In order to obtain a more detailed understanding of the consequences of NC order on the spin-density distribution of the chains, we have calculated the local $3d$ magnetic moments $\mu_d = |\langle \vec{m}_d \rangle_{\text{WS}}|$ at the Fe atoms by integrating the magnetization density inside a WS sphere of radius $r_{\text{WS}} = 1.30 \text{ \AA}$. Results for μ_d as a function of q are shown in Fig. 6 for different lattice parameters a . For large a (e.g., $a = 2.50 \text{ \AA}$) the local moments are essentially independent of q , which means that hybridization effects between the $3d$ orbitals are relatively weak in comparison with the intra-atomic Hund-rule coupling. However, the situation changes qualitatively for

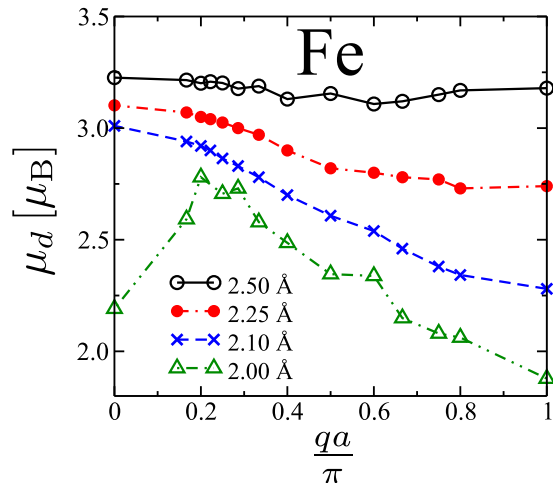


FIG. 6. Local d magnetic moments μ_d within the Wigner-Seitz spheres of Fe chains as a function of the SDW number q for different lattice parameters a .

smaller a . For $a \simeq 2.10$ – 2.25 Å one observes that μ_d decreases monotonically with increasing q . In particular for $a = 2.10$ Å, an important reduction of μ_d of about 20% is found in the AF state, as compared to that found in the FM state. At the optimal $q_{\min} \simeq 0.35\pi/a$ the reduction of μ_d is only about 10%. Remarkably, for the smallest considered $a = 2.0$ Å, μ_d shows a nonmonotonous dependence on q . It first increases with q , showing a maximum for $qa/\pi \simeq 0.2$ – 0.3 , before decreasing again as the $\pi/2$ spiral and the AF order are approached. Notice that the value of q yielding the largest μ_d is significantly smaller than $q_{\min} \simeq 0.45\pi/a$, which corresponds to the lowest energy (compare Figs. 5 and 6). The rather small unsaturated value of μ_d in the FM state for $a = 2.0$ Å is most probably a consequence of the increase of the $3d$ bandwidth as a decreases, which reduces the $3d$ -electron DOS at the Fermi energy ε_F (Stoner criterion). However, as discussed in Sec. V, the $3d$ bands tend to narrow in the spiral states as compared to the FM state. The associated enhancement of the DOS near ε_F explains the significant increase of μ_d observed for $a = 2.0$ Å and small q . A very similar behavior of μ_d has been found by using the local spin-density approximation. In this case one observes that for $a \geq 2.1$ Å μ_d decreases monotonously with increasing q , while for $a = 2.0$ Å μ_d increases for small q , reaching a maximum for $q \simeq 0.3\pi$ and then decreasing as one approaches the AF configuration. Notice, however, that the behavior might be different in other approximations to exchange and correlation, particularly in those enhancing the importance of d -electron exchange [55].

In Fig. 7 the x and y components of the magnetization density $\vec{m}(\vec{r})$ are shown for an Fe chain in a spiral state having $q = \pi/4a$. As in the case of V (Fig. 3) one observes that $m(\vec{r})$ is essentially localized within the WS spheres around the atoms, decreasing strongly in the interstitial region, where the actual change in direction of $\vec{m}(\vec{r})$ takes place. Within the WS spheres, the components $m_x(\vec{r})$ and $m_y(\vec{r})$ follow the orientation of the local moments $\vec{\mu}_i$. This can be clearly seen by comparing Figs. 7(a) and 7(b) with the illustration of the spiral state at the top of the figure. As expected, the changes in magnetization density from atom to atom correspond to simple rotations of

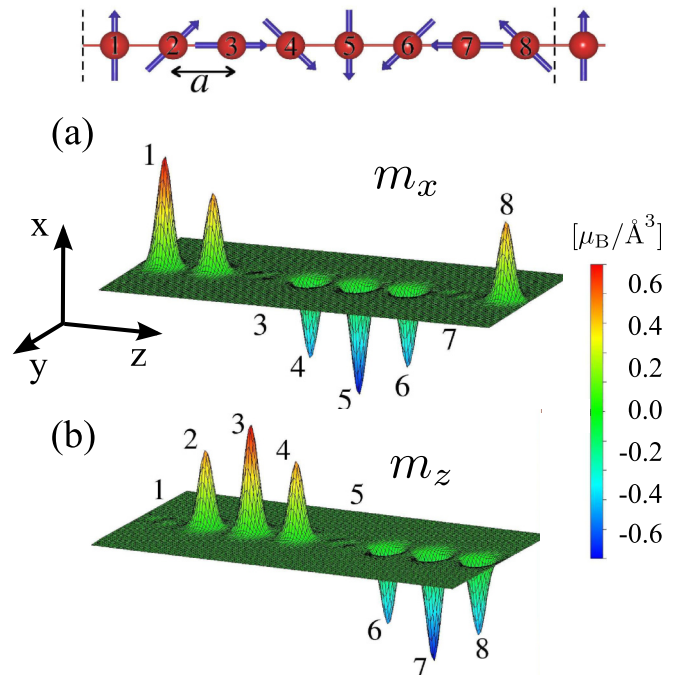


FIG. 7. Magnetization-density components (a) m_x and (b) m_z of an Fe chain in a SDW state having a wave vector $\vec{q} = (0, 0, \pi/4a)$, where $a = 2.25$ Å is the lattice parameter. The top figure illustrates the corresponding orientation of the local magnetic moments $\vec{\mu}_i$.

$\vec{m}(\vec{r})$. Notice that the calculated dominant spin-polarization is essentially symmetric around the atoms. A certain asymmetry has been observed in the STM images of Co atoms on a Mn substrate, which has been ascribed to the contribution of the underlying noncollinear Mn template [22].

IV. MAGNETIC PHASE DIAGRAMS

The discussion in the preceding section, as well as in some previous studies [14–16,41], has shown that the spiral SDW states in 1D TMs can be interpreted from a local perspective as the result of competing effective exchange interactions $J_{0\delta}$ between the local magnetic moments along the chain. It is therefore most interesting to analyze under which conditions complex NC magnetic configurations should be expected. A complete general picture of the magnetic solutions is provided by the phase diagrams of the classical 1D Heisenberg model given by Eq. (3). It is the purpose of this section to use this model in order to analyze how the changes in the lattice parameter and in the local environment of the atoms modify the interplay among the different $J_{0\delta}$ in V, Mn, and Fe chains. For simplicity, we neglect at the beginning the couplings beyond second-NNs. An analogous study has been performed in Ref. [16] in order to clarify the evolution from AF order, over spirals, to FM order as the $3d$ band filling is varied from Cr to Fe. A more complete study of the model is presented at the end of this section by incorporating the effects of third-NN interactions J_{03} .

Figure 8 shows the phase diagram of the classical 1D Heisenberg model with only first- and second-NN interactions. One distinguishes three regions corresponding to FM order

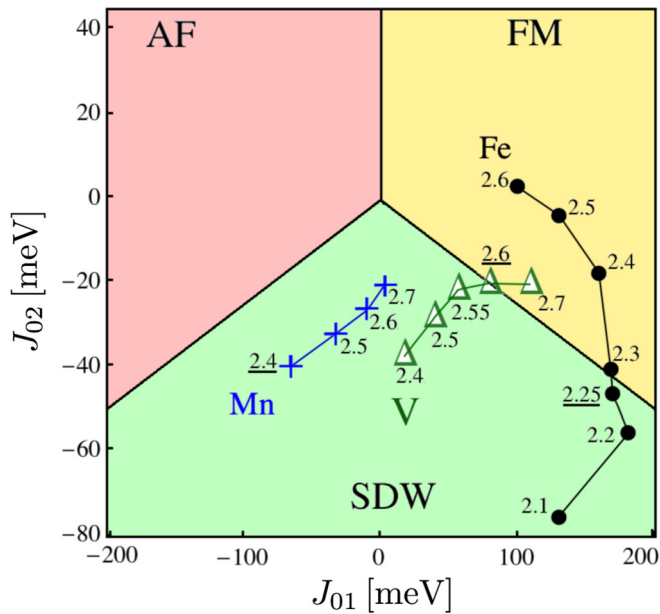


FIG. 8. Magnetic phase diagram of the classical one-dimensional Heisenberg model. The phases corresponding to ferromagnetic (FM), antiferromagnetic (AF), and spiral spin-density-wave (SDW) orders in the ground state are indicated as a function of the exchange interactions J_{01} and J_{02} between first- and second-nearest neighbors. The symbols show the effective exchange interactions J_{0s} in V, Mn, and Fe chains, as derived from the *ab initio* dispersion relations $\Delta E(q)$ for the lattice parameters a indicated in Å (see Figs. 2, 4, and 5). The equilibrium a is underlined.

($q = 0$), AF order ($q = \pi/a$), and spiral SDWs with $0 < q < \pi/a$. In the FM region $J_{01} > 0$ and either J_{01} and J_{02} do not compete (i.e., $J_{02} \geq 0$) or J_{01} dominates clearly over J_{02} (i.e., $J_{01} > 4|J_{02}|$ for $J_{02} < 0$). In the AF region $J_{01} < 0$ and either J_{01} and J_{02} do not compete (i.e., $J_{02} \geq 0$) or J_{01} dominates clearly over J_{02} (i.e., $|J_{01}| > 4|J_{02}|$ for $J_{02} < 0$). Finally, the characteristic of the NC regime is that the first- and second-NN interactions compete with comparable strengths (i.e., $|J_{01}| < 4|J_{02}|$).

The symbols shown in the diagram indicate the actual values of J_{01} and J_{02} calculated for V, Mn, and Fe chains using DFT for different lattice parameters a . Each point is obtained from an independent *ab initio* dispersion relation, like the ones discussed in the previous section. A number of important differences among the elements are revealed. In the case of V and Fe, the NN coupling J_{01} is always positive while in Mn it is negative. The second-NN exchange interaction J_{02} is found to be always negative, except in strongly stretched Fe chains with $a = 2.6$ Å. This means that J_{01} and J_{02} are always competing, either because one is FM and the other AF, or because they are both AF.

Following the evolution of the ratio J_{01}/J_{02} allow us to understand the transition from FM to SDW order in V and Fe as a function of a . For relative large NN distances (e.g., $a = 2.6$ Å) V and Fe chains show FM order, since the second-NN coupling J_{02} is relatively weak. However, as a decreases, V and Fe involve different directions. In Fe, starting from $a = 2.6$ Å, both J_{01} and $|J_{02}|$ increase at first, in a way that keeps the ratio J_{02}/J_{01} smaller than $1/4$. Therefore, FM

order remains stable. However, for $a \leq 2.4$ Å, J_{01} ceases to increase and eventually decreases somewhat for very small a . At the same time $|J_{02}|$ continues to increase monotonously as the bond length is reduced. It is the growing importance of the AF J_{02} , relative to J_{01} , that turns Fe chains into the spiral state for $a \leq 2.25$ Å (see Fig. 8). The situation is different in V chains. In this case J_{01} decreases monotonously with decreasing a , although it remains positive ($a \geq 2.4$ Å). This implies a weakening of the FM coupling with increasing hybridization and $3d$ bandwidth, which finally results in a weak antiferromagnetic NN coupling when a is very short. At the same time, $|J_{02}|$ increases ($J_{02} < 0$) stabilizing a spiral state as soon as $|J_{02}| > |J_{01}|/4$ (see Fig. 8). In contrast to V and Fe, J_{01} and J_{02} are both negative in Mn chains, with $|J_{02}| > |J_{01}|/4$ for all the considered lattice parameters (2.4 Å $\leq a \leq 2.7$ Å). Under these circumstances the magnetic order has always a spiral form. Only the periodicity of the optimal SDW and its stability relative to the collinear FM and AF configurations depend on the interatomic distance a . It would be very interesting to explore the possibility of manipulating the magnetic order in experiment, for example, by introducing stress on the chains through the substrate configuration or the field generated by an STM tip.

The electronic calculations have shown that the third-NN exchange interactions J_{03} are non-negligible in 1D systems, particularly when J_{01} and J_{02} tend to compensate. In some cases, J_{03} is comparable or even more important than the normally dominant first- and second-NN couplings. For example, in Mn we obtain $J_{01} = -2.1$ meV, $J_{02} = -23.5$ meV, and $J_{03} = 11.3$ meV in the GGA for $a = 2.7$ Å (see Fig. 4). Moreover, close to the phase boundaries of the simplest J_{01}/J_{02} model shown in Fig. 8, it is clear that the interactions at longer distances are crucial in order to remove degeneracies and determine the spin order. It is therefore interesting to extend the Heisenberg model calculations by including third-NN interactions. The corresponding magnetic phase diagram is shown in Fig. 9. Since $|J_{01}|$ defines the unit of energy, only the sign of J_{01} is relevant for the magnetic order. In this more compact form the results of Fig. 8 are recovered at the horizontal axis $J_{03} = 0$. The crossing point with the vertical line $J_{02}/|J_{01}| = -1/4$ defines the boundary between the SDW states and the collinear FM or AF orders for $J_{01} > 0$ and $J_{01} < 0$, respectively.

Introducing an additional interaction parameter renders the phase diagram a great deal richer. For $J_{01} > 0$ and very small J_{02} , one observes that the third-NN coupling J_{03} tends to stabilize a FM state (I) when positive and a SDW state (IV) when negative [see Fig. 9(a)]. On the other side, for $J_{01} < 0$ and very small J_{02} , the third-NN coupling shifts the balance in favor of the AF state (VII) for $J_{03} < 0$, or in favor of the SDW state (VI) for $J_{03} > 0$ [see Fig. 9(b)]. More important in the context of the present *ab initio* calculations for V, Mn, and Fe is the case where J_{02} is sizable and $|J_{03}|$ is not too large. As J_{02} increases, the effects of J_{03} on the magnon dispersion relations and on the ground-state order become less important. For example, the range of values of J_{03} corresponding to spiral order increases strongly with increasing $|J_{02}|$ (see Fig. 9). Although J_{03} introduces many different shapes of the dispersion relation $\Delta E(q)$, and thus several different magnetic phases, it does not change the magnetic behavior qualitatively,

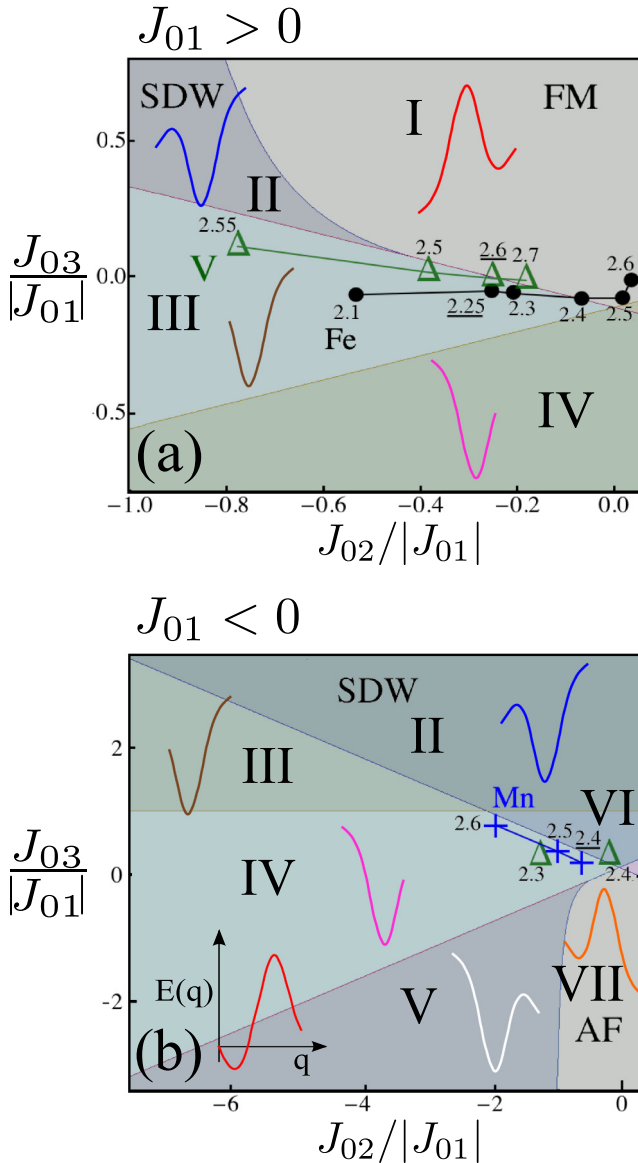


FIG. 9. Phase diagram of the one-dimensional classical Heisenberg model having exchange interactions J_{0s} up to third-NNs: (a) ferromagnetic NN coupling $J_{01} > 0$ and (b) antiferromagnetic NN coupling $J_{01} < 0$. The Roman numbers label the different types of ground-state magnetic orders and the different shapes of the magnon dispersion relations $\Delta E(q)$ as sketched: ferromagnetic order (I), spiral spin-density waves (II–VI), and antiferromagnetic order (VII). The symbols mark the actual values of J_{0s} derived from the *ab initio* frozen-magnon dispersion relations of V, Mn, and Fe chains for the lattice parameters a indicated in Å.

provided that $|J_{02}|$ is not too small. This confirms our previous conclusions based on the simpler Fig. 8.

The symbols in Fig. 9 show the results for the exchange interactions derived from the *ab initio* dispersion relations. One observes that Fe and V chains belong to the SDW region III for most lattice parameters a (i.e., $2.4 \text{ \AA} < a < 2.6 \text{ \AA}$ for V and $a < 2.4 \text{ \AA}$ for Fe). In these cases, J_{03} is approximately four times smaller than J_{02} , $-0.8 < J_{02}/|J_{01}| < 0$ and $-0.15 < J_{03}/|J_{01}| < 0.2$. The corresponding dispersion relations have

one global minimum at an intermediate q , which implies a spin-spiral configuration. The FM state is here more stable than the AF one. However, at larger interatomic distances ($a > 2.6 \text{ \AA}$ for V and $a > 2.4 \text{ \AA}$ for Fe) a transition from region III to the FM region I occurs [see Fig. 9(a)]. The exchange couplings of Mn chains belong to region IV of the phase diagram, at least for the considered lattice parameters. As in region III, $\Delta E(q)$ shows here one global minimum at an intermediate q corresponding to a spiral SDW ground state. However, the AF order is more stable than the FM state. As already observed, $|J_{02}|$ is comparable to or larger than J_{01} . Notice, moreover, that the results for J_{0s} in Mn lie close to the boundary with region II, where the ground state has a similar NC configuration, but the AF arrangement is less stable than the FM order [see Fig. 9(b)]. These differences reflect the subtle interplay between the exchange interactions at various distances. Nevertheless, the SDW order is very robust in Mn chains. Reasonable changes in the exchange couplings do not change its ground-state behavior qualitatively.

V. LOCAL ELECTRONIC STRUCTURES IN SPIN-SPIRAL STATES

The single-particle spectrum of low-dimensional systems lacking full translational symmetry can be characterized by the local density of electronic states (DOS) $\rho(\varepsilon, \vec{r}, \sigma)$ projected on the position \vec{r} and spin σ . Integrating $\rho(\varepsilon, \vec{r}, \sigma)$ for \vec{r} within the WS sphere of each atom i , one obtains the atom-resolved local DOS $\rho_{i\sigma}(\varepsilon)$. In collinear spin configurations, i.e., when the magnetization density $\vec{m}(\vec{r}) = m_z(\vec{r}) \hat{z}$ for some direction \hat{z} , there is no mixing between the spin-up and spin-down bands. Therefore, choosing \hat{z} as the spin-quantization axis, it is straightforward to distinguish the two pure spin contributions to the DOS. However, if the magnetic order is NC, the spin-up and spin-down orbitals are hybridized, and the spin components of the electronic states cannot be easily told apart. In such cases it is meaningful to take the direction of the local magnetic moment $\vec{\mu}_i$ at each atom i as the spin-quantization axis and to regard the spin-resolved local electronic structure from the perspective of this atom-specific spin direction. Indeed, the local density of states $\rho_{i\sigma}(\varepsilon)$ obtained by projecting the spinor states along $\vec{\mu}_i$ is adapted to the local symmetry. They are the same for all atoms, since the spiral SDW states are rototranslational invariant for all q . In other words, a translation of the orbital coordinates by a lattice parameter a along the wire, followed by a rotation of the spin coordinates by an angle $\theta = qa$ around the axis of the wire, leaves the electronic states unchanged. In this way, the local electronic structures of spiral states can be compared without difficulty for different q and a . In the following we present and discuss results for $\rho_{i\sigma}(\varepsilon)$ in Mn and Fe chains. Results for V chains may be found in Ref. [14].

A. Mn chains

The spin-resolved local d -electron DOS $\rho_{i\sigma}^d(\varepsilon)$ of Mn chains is shown in Fig. 10 for representative values of q and a lattice parameter $a = 2.5 \text{ \AA}$. In the FM arrangement ($q = 0$) one observes relatively narrow majority and minority d bands located, respectively, about 2.63 eV below and 1.2 eV above

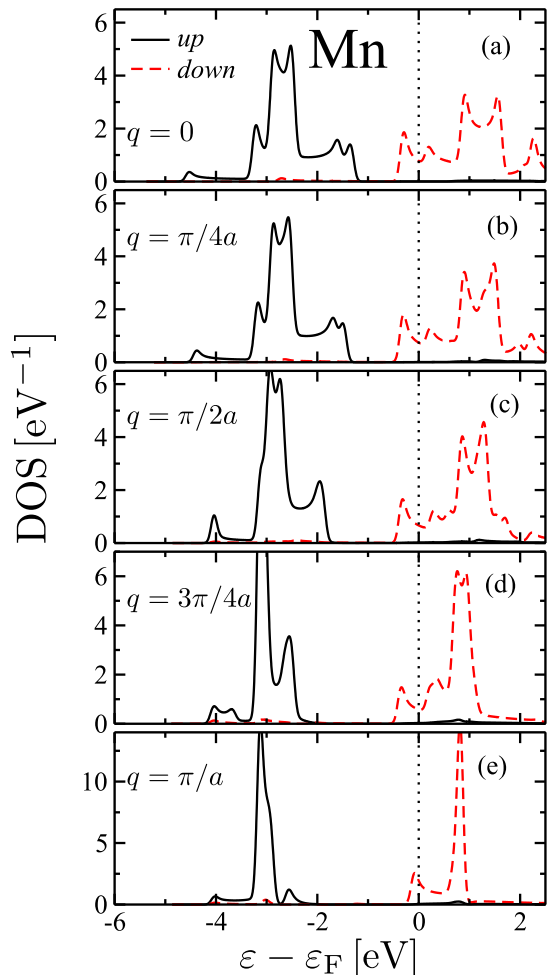


FIG. 10. Local $3d$ -electron density of states $\rho_{i\sigma}^d(\varepsilon)$ of free-standing Mn chains having a lattice parameter $a = 2.5 \text{ \AA}$ for representative SDW numbers q . Results are given for the majority-spin (black solid curves) and minority-spin (red dashed curves) components along the direction of the local magnetic moment $\vec{\mu}_i$. The Fermi energy ε_F is indicated by the vertical dotted line.

the Fermi level ε_F . The exchange splitting between the local majority- and minority-spin states is about 3.8 eV , while the calculated local magnetic moment per atom is $\mu = 3.94\mu_B$. As q increases in NC spin arrangements, several major qualitative changes in $\rho_{i\sigma}^d(\varepsilon)$ are observed. The noncollinearity implies that the spin projection is no longer a good quantum number. Thus, majority- and minority-spin orbitals hybridize. The hopping integrals between the local majority orbitals of one atom and the minority orbitals of a neighboring atom increase with q , reaching a maximum in the AF state. Conversely, the NN hoppings between the local majority-spin directions and between the local minority-spin directions, which are not the same except for $q = 0$, decrease with increasing q . They are maximal for $q = 0$ and vanish between nearest neighbors for $q = \pi/a$. The resulting spin mixing alters significantly the electronic structure as a function of q . First of all one observes that the hybridization between different local spin directions causes a level repulsion, which shifts the majority (minority) bands to lower (higher) energies. This is a consequence of the clear en-

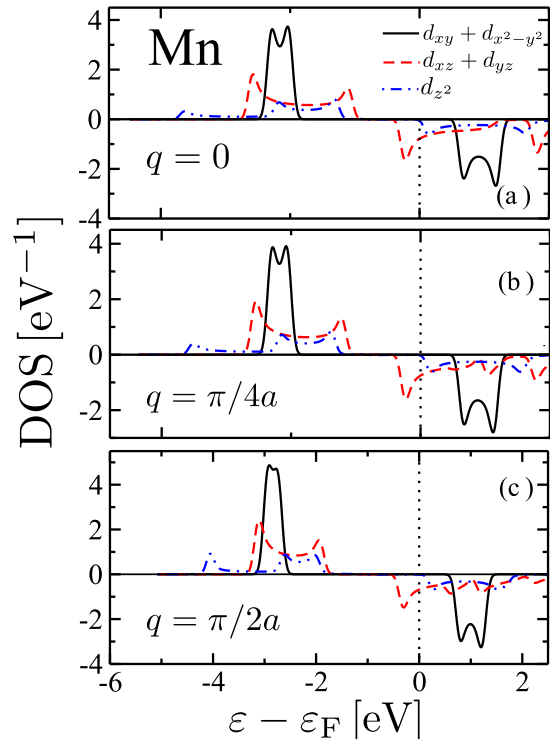


FIG. 11. Orbital-resolved density of states $\rho_{i\alpha\sigma}(\varepsilon)$ of free-standing Mn chains having a lattice parameter $a = 2.5 \text{ \AA}$ and representative wave numbers q : (a) $q = 0$, (b) $q = \pi/4a$, and (c) $q = \pi/2a$. Positive (negative) values correspond to the majority (minority) spin-direction taking the spin-quantization axis along the local magnetic moment $\vec{\mu}_i$. The Fermi energy ε_F is indicated by the vertical dotted line.

ergy separation between the local majority- and minority-spin orbitals due to the exchange splitting. Depending on the $3d$ -band filling, this contributes to lowering the band energy of the chains. The second important consequence of increasing q is a substantial reduction on the $3d$ bandwidth W_d , together with a shift in the position of the peaks of both majority and minority bands. In the examples shown in Fig. 10 we find $W_d = 3.5, 3.2, 2.5, 2.0$, and 1.8 eV for $q = 0, \pi/4a, \pi/2a, 3\pi/4a$, and π/a , respectively. The average density of states within the $3d$ bands increases accordingly. The changes in the local electronic structure as a function of q and the band-narrowing effects are also clearly observed in the integrated DOS, which gives the number of $3d$ electrons as a function of the Fermi energy [54].

The orbital-resolved DOS $\rho_{i\alpha\sigma}(\varepsilon)$ shown in Fig. 11 provides more detailed information of the electronic structure as a function of SDW number q . Assuming that the chain is along the z direction, the $3d$ orbitals can be grouped into the $dd\sigma$ band, given by the $d_{3z^2-r^2}$ orbitals, the doubly degenerated $dd\pi$ band, including the d_{xz} and d_{yz} orbitals, and the doubly degenerated $dd\delta$ band, including the $d_{x^2-y^2}$ and d_{xy} orbitals. In the absence of spin-orbit interactions these bands are decoupled. The largest bandwidth corresponds, as expected, to the σ orbitals, which point along the NN bonds, followed by the π bands and finally the δ bands. The exchange splitting between majority and minority states is in all cases very important and approximately independent of q . This reflects

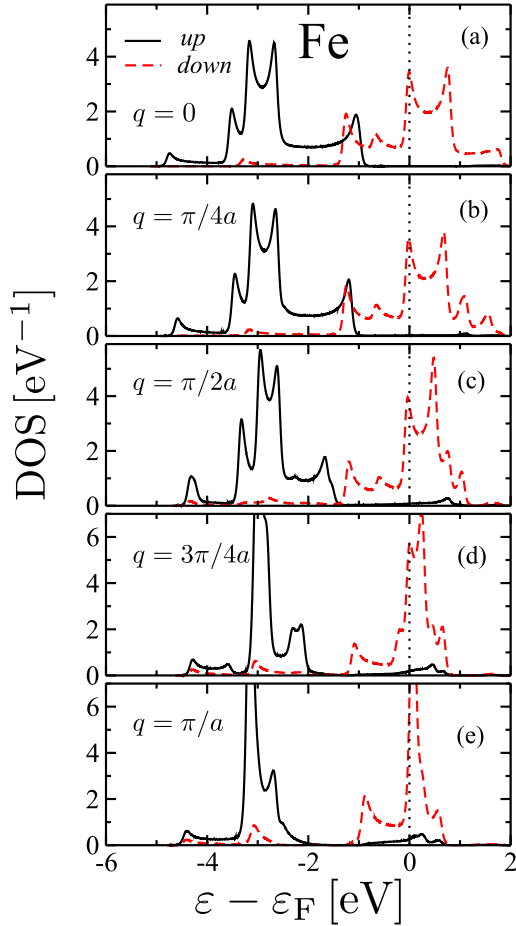


FIG. 12. Local 3d-electron density of states (DOS) $\rho_{i\sigma}^d(\varepsilon)$ of free-standing Fe chains having a NN distance $a = 2.25 \text{ \AA}$ for representative SDW numbers q . Results are given for the majority-spin (black solid curves) and minority-spin (red dashed curves) components along the direction of the local magnetic moment $\bar{\mu}_i$. The Fermi energy ε_F is indicated by the vertical dotted lines.

the large stability of the local Mn moments. However, the bandwidths are significantly reduced as q increases. Let us recall that the spin component of the local density of states shown in Figs. 10 and 11 are projected along the local majority- and minority-spin directions of a given atom. For a comparison with spin-polarized scanning tunneling spectroscopy (STS) measurements, the orientation of the local moments along the chain relative to the tip magnetization has to be taken into account [22].

B. Fe chains

The spin-resolved local 3d DOS of Fe chains having a lattice parameter $a = 2.25 \text{ \AA}$ are shown in Fig. 12 for different wave numbers q . In this case, owing to the larger bandwidth and the somewhat smaller exchange splitting, we find that the majority and minority bands overlap to some extent (for about 1 eV) in the FM state. As q increases, one observes the narrowing of the majority- and minority-spin bands, as well as the shift of the majority-spin (minority-spin) peaks to lower (higher) energies. In particular, we find that the 3d bandwidth amounts to $W_d = 3.61, 3.48, 2.94, 2.56, \text{ and } 2.47 \text{ eV}$ for $q = 0,$

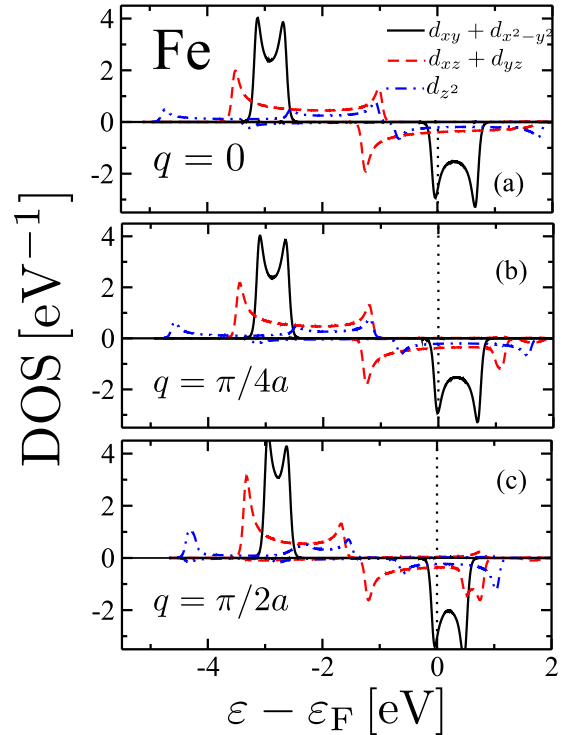


FIG. 13. Orbital-resolved density of states $\rho_{i\alpha\sigma}(\varepsilon)$ of free-standing Fe chains having a lattice parameter $a = 2.25 \text{ \AA}$ and representative wave numbers q : (a) $q = 0$, (b) $q = \pi/4a$, and (c) $q = \pi/2a$. Positive (negative) values correspond to the majority (minority) spin direction taking the spin-quantization axis along the local magnetic moment $\bar{\mu}_i$. The Fermi energy ε_F is indicated by the vertical dotted line.

$\pi/4a, \pi/2a, 3\pi/2a,$ and π/a , respectively. Qualitatively, these trends are analogous to the case of Mn chains. However, in the case of Fe the consequences of band narrowing are more striking, since they imply the opening of a gap in the occupied single-particle spectrum as q increases (see Fig. 12). This behavior could, in principle, be investigated by means of STS measurements.

More detailed information on the electronic structure of Fe chains is provided by the orbital-resolved DOS $\rho_{i\alpha\sigma}(\varepsilon)$, which is shown in Fig. 13 for representative values of q . As in the case of Mn, due to the symmetry of the chains along the z direction, and in the absence of spin-orbit coupling, the 3d orbitals lead to three bands: the $dd\sigma$ band formed by the $d_{3z^2-r^2}$ orbitals, the doubly degenerated $dd\pi$ band formed by the d_{xz} and d_{yz} orbitals, and the doubly degenerated $dd\delta$ band formed by the $d_{x^2-y^2}$ and d_{xy} orbitals. For $q = 0$, one observes the characteristic FM exchange splitting between up and down local densities of states. The different bandwidths of the subbands reflect the orientation of the corresponding d orbitals with respect to the wire. On the one side, the $dd\delta$ bands have the smallest bandwidth (approximately 0.6 eV) since the xy and x^2-y^2 orbitals are perpendicular to the chain. On the other side, the width of the $dd\sigma$ band is the largest, since the orbitals point along the chain direction. These orbitals are, in fact, responsible for the overlap between majority and minority bands for $q = 0$. Concerning the dependence on q , we find that

all bands are affected by the narrowing effect as q increases (see Fig. 13).

VI. CONCLUSION

The electronic and magnetic properties of $3d$ TM chains showing spiral SDW states have been investigated by combining first-principles methods and phenomenological approaches. One observes that V, Mn, and Fe chains develop stable spin-spiral arrangements at their equilibrium distances. Bond-length reduction tends to further stabilize NC spin arrangements, while expansion tends to favor collinear FM order. This could allow some degree of manipulation of the magnetic order in point contacts or by strain induced upon deposition on different substrates.

A local analysis of the magnetic properties has been performed by deriving the effective exchange interactions J_{0s} between the local moments from the *ab initio* frozen-magnon dispersion relations $\Delta E(q)$ for different lattice parameters a . In most cases, the stability of the NC magnetic arrangements is essentially the result of competing first- and second-NN interactions J_{01} and J_{02} . However, third-NN interactions were found to play a significant role when the usually dominant J_{01} and J_{02} compensate each other, or when one of them nearly vanishes. The changes in the magnetic order of the chains as a function of a have been analyzed in the framework of a classical Heisenberg model with competing interactions. This allowed us to classify under which circumstances (i.e., values of J_{0s}) a given magnetic order corresponds to the most stable configuration.

The consequences of the spiral magnetic order on the electronic structure of the chains has been quantified by computing the wave-number dependence of the local density of electronics states. Band-narrowing and level-repulsion effects have been identified as a function of q . The depletion of the $3d$ -electron DOS around the Fermi energy, along with the strong hybridization between the orbitals having opposite spin directions, explains qualitatively the stability of the NC magnetic configurations.

Among the future perspectives of this work one should mention studies of $3d$ TM chains, wires, and stripes deposited on metallic and insulating substrates of experimental interest. In this case, additional magnetic interactions, for example, those mediated by the substrate or the transversal interactions across finite width wires, would come into play. They are likely to alter the competition between exchange couplings at different distances, which has been discussed in this work,

and could therefore affect the stability of the spin-spiral configurations, as already observed in the case of Mn on Cu(110) and Ag(110) [16]. In this way the magnetic order could be investigated as a function of the width of the wire or stripe on which some theoretical and experimental results are available [1,41]. Another interesting aspect is to investigate in more detail how the magnetic order of the chains depends on electron-correlation effects, by considering alternative approximations to the exchange-correlation energy functional. For example, introducing parameterized local interactions in the Hartree-Fock approximation, as in the LDA + U method [55], is likely to enhance even further the stability of the local magnetic moments, thus reducing their dependence on the SDW number q . Depending on band filling, a larger stability of the FM order or a reduction of NN antiferromagnetic couplings could follow, which could modify the stability of the spiral SDWs or at least their optimal wave number q_{\min} . A dynamical treatment of Coulomb interactions following dynamical mean-field theory [56] appears as a most worthwhile evolution in this context, since the magnetic order and effective magnetic interaction in transition-metal chains and wires are known to be the result of a subtle interplay between kinetic and Coulomb energies in a low-dimensional environment. Furthermore, the stability of the SDWs should be investigated by taking into account spin-orbit interactions, particularly for $3d$ - $4d$ and $3d$ - $5d$ alloy wires, as well as for $3d$ wires deposited on highly polarizable $4d$ and $5d$ substrates. Indeed, the interplay between NC magnetic order and spin-orbit coupling in structures lacking inversion symmetry (e.g., deposited chains and stripes) should give rise to interesting chiral effects which deserve detailed investigation. Finally, from a somewhat different perspective, the exchange couplings J_{ij} between the local moments, which were obtained in the present static DFT calculations, could be useful in order to explore the dynamical magnetic properties of 1D systems. They could also help to shed light on more complex 2D or 3D magnetic structures, such as domain walls, which are important for technological applications.

ACKNOWLEDGMENTS

This work has been supported by the Deutscher Akademischer Austausch Dienst (DAAD) and by the Deutsche Forschungsgemeinschaft (DFG). Computer resources provided by the IT Service Center of the University of Kassel and by the Center for Scientific Computing of the University of Frankfurt are gratefully acknowledged.

-
- [1] P. Gambardella, A. Dallmeyer, K. Maiti, M. C. Malagoli, W. Eberhardt, K. Kern, and C. Carbone, Ferromagnetism in one-dimensional monatomic metal chains, *Nature (London)* **416**, 301 (2002); P. Gambardella, M. Blanc, H. Brune, K. Kuhnke, and K. Kern, One-dimensional metal chains on Pt vicinal surfaces, *Phys. Rev. B* **61**, 2254 (2000).
 - [2] J. Shen, R. Skomski, M. Klaua, H. Jenniches, S. S. Manoharan, and J. Kirschner, Magnetism in one dimension: Fe on Cu(111), *Phys. Rev. B* **56**, 2340 (1997).
 - [3] G. A. Prinz, Magnetoelectronics, *Science* **282**, 1660 (1998).
 - [4] D. A. Allwood, G. Xiong, C. C. Faulkner, D. Atkinson, D. Petit, and R. P. Cowburn, Magnetic domain-wall logic, *Science* **309**, 1688 (2005).
 - [5] L. Hammer, W. Meier, A. Schmidt, and K. Heinz, Submonolayer iron film growth on reconstructed Ir(100)-(5 × 1), *Phys. Rev. B* **67**, 125422 (2003); L. Hammer, W. Meier, A. Klein, P. Landfried, A. Schmidt, and K. Heinz, Hydrogen-Induced

- Self-Organized Nanostructuring of the Ir(100) Surface, *Phys. Rev. Lett.* **91**, 156101 (2003).
- [6] K. Tsukagoshi, B. W. Alphenaar, and H. Ago, Coherent transport of electron spin in a ferromagnetically contacted carbon nanotube, *Nature (London)* **401**, 572 (1999).
- [7] V. Rodrigues, J. Bettini, P. C. Silva, and D. Ugarte, Evidence for Spontaneous Spin-Polarized Transport in Magnetic Nanowires, *Phys. Rev. Lett.* **91**, 096801 (2003).
- [8] S. A. Wolf, D. D. Awschalom, R. A. Buhrman, J. M. Daughton, S. von Molnár, M. L. Roukes, A. Y. Chtchelkanova, and D. M. Treger, Spintronics: A spin-based electronics vision for the future, *Science* **294**, 1488 (2001).
- [9] H. Ohno, A window on the future of spintronics, *Nat. Mater.* **9**, 952 (2010).
- [10] J. Dorantes-Dávila and G. M. Pastor, Magnetic Anisotropy of One-Dimensional Nanostructures of Transition Metals, *Phys. Rev. Lett.* **81**, 208 (1998).
- [11] Y. Mokrousov, G. Bihlmayer, S. Blügel, and S. Heinze, Magnetic order and exchange interactions in monoatomic *3d* transition-metal chains, *Phys. Rev. B* **75**, 104413 (2007).
- [12] V. S. Stepanyuk, L. Niebergall, R. C. Longo, W. Hergert, and P. Bruno, Magnetic nanostructures stabilized by surface-state electrons, *Phys. Rev. B* **70**, 075414 (2004).
- [13] P. Ferriani, K. von Bergmann, E. Y. Vedmedenko, S. Heinze, M. Bode, M. Heide, G. Bihlmayer, S. Blügel, and R. Wiesendanger, Atomic-Scale Spin Spiral with a Unique Rotational Sense: Mn Monolayer on W(001), *Phys. Rev. Lett.* **101**, 027201 (2008).
- [14] M. Saubanère, M. Tanveer, P. Ruiz-Díaz, and G. M. Pastor, First principles theoretical study of complex magnetic order in transition-metal nanowires, *Phys. Status Solidi B* **247**, 2610 (2010).
- [15] J. C. Tung and G. Y. Guo, *Ab initio* studies of spin-spiral waves and exchange interactions in *3d* transition metal atomic chains, *Phys. Rev. B* **83**, 144403 (2011).
- [16] F. Schubert, Y. Mokrousov, P. Ferriani, and S. Heinze, Non-collinear magnetism in freestanding and supported monatomic Mn chains, *Phys. Rev. B* **83**, 165442 (2011).
- [17] H. Oka, O. O. Brovko, M. Corbetta, V. S. Stepanyuk, D. Sander, and J. Kirschner, Spin-polarized quantum confinement in nanostructures: Scanning tunneling microscopy, *Rev. Mod. Phys.* **86**, 1127 (2014).
- [18] S. Lounis, P. H. Dederichs, and S. Blügel, Magnetism of Nanowires Driven by Novel Even-Odd Effects, *Phys. Rev. Lett.* **101**, 107204 (2008).
- [19] R. N. Igarashi, A. B. Klautau, R. B. Muniz, B. Sanyal, and H. M. Petrilli, First-principles studies of complex magnetism in Mn nanostructures on the Fe(001) surface, *Phys. Rev. B* **85**, 014436 (2012).
- [20] H. Roeder, E. Hahn, H. Brune, J.-P. Bucher, and K. Kern, Building one- and two-dimensional nanostructures by diffusion-controlled aggregation at surfaces, *Nature (London)* **366**, 141 (1993).
- [21] N. N. Negulyaev, V. S. Stepanyuk, L. Niebergall, P. Bruno, W. Hergert, J. Repp, K. H. Rieder, and G. Meyer, Direct Evidence for the Effect of Quantum Confinement of Surface-State Electrons on Atomic Diffusion, *Phys. Rev. Lett.* **101**, 226601 (2008).
- [22] D. Serrate, P. Ferriani, Y. Yoshida, S.-W. Hla, M. Menzel, K. von Bergmann, S. Heinze, A. Kubetzka, and R. Wiesendanger, Imaging and manipulating the spin direction of individual atoms, *Nat. Nanotechnol.* **5**, 350 (2010).
- [23] M. Menzel, Y. Mokrousov, R. Wieser, J. E. Bickel, E. Vedmedenko, S. Blügel, S. Heinze, K. von Bergmann, A. Kubetzka, and R. Wiesendanger, Information Transfer by Vector Spin Chirality in Finite Magnetic Chains, *Phys. Rev. Lett.* **108**, 197204 (2012).
- [24] M. Menzel, A. Kubetzka, K. von Bergmann, and R. Wiesendanger, Parity Effects in 120° Spin Spirals, *Phys. Rev. Lett.* **112**, 047204 (2014).
- [25] L. Udvardi, L. Szunyogh, K. Palotás, and P. Weinberger, First-principles relativistic study of spin waves in thin magnetic films, *Phys. Rev. B* **68**, 104436 (2003).
- [26] M. Heide, G. Bihlmayer, and S. Blügel, Dzyaloshinskii-Moriya interaction accounting for the orientation of magnetic domains in ultrathin films: Fe/W(110), *Phys. Rev. B* **78**, 140403 (2008).
- [27] S. Mankovsky, S. Bornemann, J. Minár, S. Polesya, H. Ebert, J. B. Staunton, and A. I. Lichtenstein, Effects of spin-orbit coupling on the spin structure of deposited transition-metal clusters, *Phys. Rev. B* **80**, 014422 (2009).
- [28] S. Heinze, K. von Bergmann, M. Menzel, J. Brede, A. Kubetzka, R. Wiesendanger, G. Bihlmayer, and S. Blügel, Spontaneous atomic-scale magnetic skyrmion lattice in two dimensions, *Nat. Phys.* **7**, 713 (2011).
- [29] R. H. Liu, W. L. Lim, and S. Urazhdin, Dynamical Skyrmion State in a Spin Current Nano-Oscillator with Perpendicular Magnetic Anisotropy, *Phys. Rev. Lett.* **114**, 137201 (2015).
- [30] R. Lizárraga, L. Nordström, L. Bergqvist, A. Bergman, E. Sjöstedt, P. Mohn, and O. Eriksson, Conditions for Non-Collinear Instabilities of Ferromagnetic Materials, *Phys. Rev. Lett.* **93**, 107205 (2004).
- [31] I. E. Dzialoshinskii, Thermodynamic theory of “Weak” ferromagnetism in antiferromagnetic substances, *Sov. Phys. JETP* **5**, 1259 (1957); T. Moriya, Anisotropic superexchange interaction and weak ferromagnetism, *Phys. Rev.* **120**, 91 (1960).
- [32] L. M. Sandratskii, Noncollinear magnetism in itinerant-electron systems: Theory and applications, *Adv. Phys.* **47**, 91 (1998).
- [33] E. Sjöstedt and L. Nordström, Non-collinear full-potential studies of γ -Fe, *Phys. Rev. B* **66**, 014447 (2002).
- [34] K. Knöpfle, L. M. Sandratskii, and J. Kübler, Spin spiral ground state of γ -Fe, *Phys. Rev. B* **62**, 5564 (2000).
- [35] R. Hafner, D. Spišák, R. Lorenz, and J. Hafner, Magnetic ground state of Cr in density-functional theory, *Phys. Rev. B* **65**, 184432 (2002).
- [36] K. Nakamura, N. Mizuno, T. Akiyama, T. Ito, and A. J. Freeman, Spin-spiral structures in free-standing Fe(110) monolayers, *J. Appl. Phys.* **99**, 08N501 (2006).
- [37] T. Shimada, J. Okuno, and T. Kitamura, *Ab initio* study of spin-spiral noncollinear magnetism in a free-standing Fe(110) monolayer under in-plane strain, *Phys. Rev. B* **85**, 134440 (2012).
- [38] M. Zelený, M. Šob, and J. Hafner, Non-collinear magnetism in manganese nanostructures, *Phys. Rev. B* **80**, 144414 (2009).
- [39] C. Ataca, S. Cahangirov, E. Durgun, Y. R. Jang, and S. Ciraci, Structural, electronic, and magnetic properties of *3d* transition metal monatomic chains: First-principles calculations, *Phys. Rev. B* **77**, 214413 (2008).

- [40] M. Zelený, M. Šob, and J. Hafner, *Ab initio* density functional calculations of ferromagnetism in low-dimensional nanostructures: From nanowires to nanorods, *Phys. Rev. B* **79**, 134421 (2009).
- [41] M. Tanveer, P. Ruiz-Díaz, and G. M. Pastor, Environment-dependent noncollinear magnetic orders and spin-wave spectra of Fe chains and stripes, *Phys. Rev. B* **87**, 075426 (2013).
- [42] T. R. Dasa, P. A. Ignatiev, and V. S. Stepanyuk, Effect of the electric field on magnetic properties of linear chains on a Pt(111) surface, *Phys. Rev. B* **85**, 205447 (2012).
- [43] M. M. Bezerra-Neto, M. S. Ribeiro, B. Sanyal, A. Bergman, R. B. Muniz, O. Eriksson, and A. B. Klautau, Complex magnetic structure of clusters and chains of Ni and Fe on Pt(111), *Sci. Rep.* **3**, 3054 (2013).
- [44] G. Kresse and J. Furthmüller, Efficient iterative schemes for *Ab initio* total-energy calculations using a plane-wave basis set, *Phys. Rev. B* **54**, 11169 (1996); G. Kresse and D. Joubert, From ultrasoft pseudopotentials to the projector augmented-wave method, *ibid.* **59**, 1758 (1999).
- [45] Y. Wang and J. P. Perdew, Correlation hole of the spin-polarized electron gas, with exact small-wave-vector and high-density scaling, *Phys. Rev. B* **44**, 13298 (1991); J. P. Perdew and Y. Wang, Accurate and simple analytic representation of the electron-gas correlation energy, *ibid.* **45**, 13244 (1992); J. P. Perdew, J. A. Chevary, S. H. Vosko, K. A. Jackson, M. R. Pederson, D. J. Singh, and Carlos Fiolhais, Atoms, molecules, solids, and surfaces: Applications of the generalized gradient approximation for exchange and correlation, *ibid.* **46**, 6671 (1992).
- [46] D. M. Ceperley and B. J. Alder, Ground State of the Electron Gas by a Stochastic Method, *Phys. Rev. Lett.* **45**, 566 (1980).
- [47] S. H. Vosko, L. Wilk, and M. Nusair, Accurate spin-dependent electron liquid correlation energies for local spin density calculations: A critical analysis, *Can. J. Phys.* **58**, 1200 (1980).
- [48] P. E. Blöchl, Projector augmented-wave method, *Phys. Rev. B* **50**, 17953 (1994).
- [49] H. J. Monkhorst and J. D. Pack, Special points for Brillouin-zone integrations, *Phys. Rev. B* **13**, 5188 (1976).
- [50] D. Hobbs, G. Kresse, and J. Hafner, Fully unconstrained non-collinear magnetism within the projector augmented-wave method, *Phys. Rev. B* **62**, 11556 (2000).
- [51] P. D. Haynes and M. C. Payne, Corrected penalty-functional method for linear-scaling calculations within density-functional theory, *Phys. Rev. B* **59**, 12173 (1999).
- [52] W. Kohn, Density Functional and Density Matrix Method Scaling Linearly with The Number of Atoms, *Phys. Rev. Lett.* **76**, 3168 (1996).
- [53] P. H. Dederichs, S. Blügel, R. Zeller, and H. Akai, Ground States of Constrained Systems: Application to Cerium Impurities, *Phys. Rev. Lett.* **53**, 2512 (1984).
- [54] See Supplemental Material at <http://link.aps.org/supplemental/10.1103/PhysRevB.94.094403> where additional results on Mn chains are provided.
- [55] V. I. Anisimov, J. Zaanen, and O. K. Andersen, Band theory and Mott insulators: Hubbard U instead of Stoner I, *Phys. Rev. B* **44**, 943 (1991); A. I. Liechtenstein, V. I. Anisimov, and J. Zaanen, Density-functional theory and strong interactions: Orbital ordering in Mott-Hubbard insulators, *ibid.* **52**, R5467 (1995); V. I. Anisimov, F. Aryasetiawan, and A. I. Liechtenstein, First-principles calculations of the electronic structure and spectra of strongly correlated systems: The LDA + U method, *J. Phys.: Condens. Matter* **9**, 767 (1997).
- [56] G. Kotliar, S. Y. Savrasov, K. Haule, V. S. Oudovenko, O. Parcollet, and C. A. Marianetti, Electronic structure calculations with dynamical mean-field theory, *Rev. Mod. Phys.* **78**, 865 (2006).